ResearchGate

See discussions, stats, and author profiles for this publication at: https://www.researchgate.net/publication/256850085

Toward near real-time monitoring of forest disturbance by fusion of MODIS and Landsat data

Article *in* Remote Sensing of Environment · August 2013

DOI: 10.1016/j.rse.2013.04.002

CITATIONS
122

READS
1,723

5 authors, including:

Qinchuan Xin
Sun Yat-Sen University
80 PUBLICATIONS **2,309** CITATIONS
SEE PROFILE

Pontus Olofsson
Boston University
71 PUBLICATIONS **5,628** CITATIONS
SEE PROFILE

Zhe Zhu
University of Connecticut
85 PUBLICATIONS **12,781** CITATIONS
SEE PROFILE

Curtis E. Woodcock
Boston University
292 PUBLICATIONS **40,629** CITATIONS
SEE PROFILE

Some of the authors of this publication are also working on these related projects:

Toward Near Real-time Monitoring and Characterization of Land Surface Change for the Conterminous US View project

Land Change Monitoring, Assessment, and Project (LCMAP) View project

All content following this page was uploaded by Pontus Olofsson on 01 October 2019.

The user has requested enhancement of the downloaded file.

Remote Sensing of Environment 135 (2013) 234–247

Contents lists available at SciVerse ScienceDirect

Remote Sensing of Environment

journal homepage: www.elsevier.com/locate/rse

Toward near real-time monitoring of forest disturbance by fusion of MODIS and Landsat data

Qinchuan Xin [a,b,*], Pontus Olofsson [b], Zhe Zhu [b], Bin Tan [c], Curtis E. Woodcock [b]

[a] Ministry of Education Key Laboratory for Earth System Modeling, Center for Earth System Science, Tsinghua University, Beijing 100084, China
[b] Department of Earth and Environment, Boston University, Boston, MA 02215, USA
[c] NASA Goddard Space Flight Center Code 614.5, Greenbelt, MD 20770, USA

ARTICLE INFO

Article history:
Received 22 September 2012
Received in revised form 4 April 2013
Accepted 6 April 2013

Keywords:
MODIS
Landsat
Fusion
Time-series
Real-time
Change detection
Land change
Forest disturbance
Point spread function

ABSTRACT

Timely and accurate monitoring of forest disturbance is essential to help us understand how the Earth system is changing. MODIS (Moderate Resolution Imaging Spectroradiometer) imagery and subsequent MODIS products provide near-daily global coverage and have transformed the ways we study and monitor the Earth. To monitor forest disturbance, it is necessary to be able to compare observations of the same place from different times, but this is a challenging task using MODIS data as observations from different days have varying view angles and pixel sizes, and cover slightly different areas. In this paper, we propose a method to fuse MODIS and Landsat data in a way that allows for near real-time monitoring of forest disturbance. The method is based on using Landsat time-series images to predict the next MODIS image, which forms a stable basis for comparison with new MODIS acquisitions. The predicted MODIS images represent what the surface should look like assuming no disturbance, and the difference in the spectral signatures between predicted and observed MODIS images becomes the "signal" used for detecting forest disturbance. The method was able to detect subpixel forest disturbance with a producer's accuracy of 81% and a user's accuracy of 90%. Patches of forest disturbance as small as 5 to 7 ha in size were detected on a daily basis. The encouraging results indicate that the presented fusion method holds promise for improving monitoring of forest disturbance in near real-time.
© 2013 Elsevier Inc. All rights reserved.

1. Introduction

Changes in forests influence various aspects of the Earth system, including the climate through the exchange of carbon dioxide with the atmosphere and energy and water exchanges between the biosphere and atmosphere (DeFries et al., 1999). Most forest change is caused by natural forces such as flooding, drought, fire, insects, and diseases, or by human activities such as clear cutting, thinning, and burning (Gong & Xu, 2003). Most human-induced forest disturbances tend to be small in size (Kuemmerle et al., 2007; Townshend & Justice, 1988) and can occur within days or weeks. Timely and accurate monitoring of forest disturbance, especially human-induced disturbance, is vital to understand how the Earth is changing and the role humans are playing in that change (Hansen et al., 2008b).

Remotely sensed data from satellites have been successfully used to quantify rates of forest disturbances (Coppin et al., 2004; Singh, 1989), particularly with Landsat imagery (e.g. Kennedy et al., 2010; Masek et al., 2008). Despite tremendous progress in this domain, almost all the efforts to date have been retrospective, or quantifying past changes in the landscape. While knowledge of past locations and rates of land surface change are useful and important, another way to significantly increase the value of information about forest disturbance from remote sensing would be to provide the information as close in time as possible to when changes occur. The ability to map forest disturbances in near real-time is relevant to policy and management, as early warning allows governments to take faster action to stop illegal logging or encroachment on protected areas (INPE, 2002).

To date, what is missing is a comprehensive way to monitor forest disturbance globally in near real-time at spatial scales that will capture human activities. Use of a single satellite sensor is often limited by the trade-off between the spatial, spectral and temporal resolution of instruments. For example, moderate resolution sensors like Landsat (or similar sensing systems like CBERS, ResourceSat, SPOT/HRV, etc.) have sufficient spectral bands and fine spatial resolution that allow for accurate change detection, but simply do not collect images frequently enough for near real-time monitoring. On the other hand, MODIS (or similar sensing systems like ENVISAT/MERIS, SPOT/VGT, Suomi-NPP/VIIRS, etc.) has sufficient temporal resolution but less than ideal spatial resolution (0.25–1 km). As a result, while MODIS data have proven useful in near real-time monitoring of natural disturbance at large scales such as fires (Roy et al., 2005), insect outbreaks (Spruce et al., 2011) and drought (Verbesselt et al., 2012), most human modifications to the environments, particularly over days to weeks,

* Corresponding author at: Ministry of Education Key Laboratory for Earth System Modeling, Center for Earth System Science, Tsinghua University, Beijing 100084, China. Tel.: +86 188 1025 3088.
E-mail address: xqcchina@gmail.com (Q. Xin).

0034-4257/$ – see front matter © 2013 Elsevier Inc. All rights reserved.
http://dx.doi.org/10.1016/j.rse.2013.04.002

are considerably smaller. In addition, most analysis to date has been retrospective or quantifying changes in the landscape in yearly or decadal time steps (Carroll et al., 2004; Zhan et al., 2002). So far, neither Landsat nor MODIS, by themselves, have been capable of forming the basis for global monitoring of forest disturbance in near real-time.

1.1. The difficulties of using MODIS data to monitor forest disturbance

To capture abrupt disturbances, it is necessary to compare frequent observations of the same place (Lhermitte et al., 2011). However, per-pixel comparison of MODIS daily imagery has proven problematic because a substantial proportion of the spectral signal of each MODIS pixel comes from surrounding areas (Townshend et al., 2000). Fig. 1 shows the footprints of one week of MODIS observations overlaid on a QuickBird image (methods described in Section 3.2). Although the footprints vary considerably in size and center locations, and cover a diverse set of land covers, they are binned into the same predefined grid cell (the white parallelogram in Fig. 1) to produce downstream products (Wolfe et al., 1998). On average, only about 30% of the MODIS observations come from the area of the associated grid cell (Tan et al., 2006).

The result is high variability in the spectral signatures on consecutive days, which complicates monitoring of changes (Fig. 2). For example, the surface reflectance on Day 258 and 260 is lower than that on Day 255, simply because of the spectral contribution from a small pond (dark blue area in Fig. 1). This illustrates the reason it is difficult to monitor land change with MODIS daily gridded products: the spectral signatures associated with the same grid cell can change significantly even when the land surface is not changing.

The impact of the mismatch between MODIS swath observations and predefined grid cells is known (Huang et al., 2002) and has been documented by Roy (2000) with implications being explored by Tan et al. (2006). For these reasons, it is a common practice to use composited MODIS data or averages over time and/or space to minimize this noise (e.g. Jin & Sader, 2005; Lunetta et al., 2006). As such, existing efforts that use MODIS gridded data for change detection have tended to focus on large changed patches and have largely been retrospective. However, given the relatively small sizes of most land changes (Townshend & Justice, 1988), particularly at time scales of days to weeks, it is essential to be able to process MODIS daily data at pixel level to find areas of forest disturbance.

1.2. Fusion of Landsat and MODIS data

One possible solution to this problem is to combine the strengths of the high spatial resolution of Landsat and the high temporal resolution of MODIS. There has been progress in the blending of Landsat and

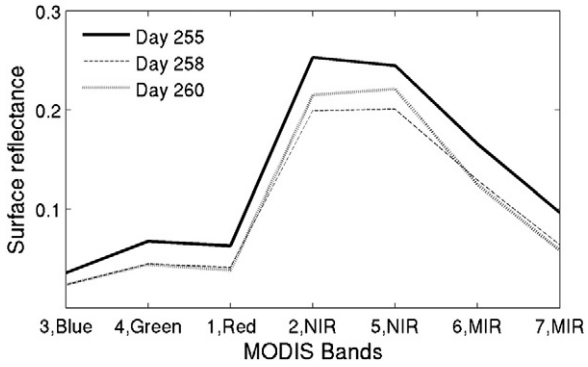

Fig. 2. The spectral signatures of cloud-free observations shown in Fig. 1. Note that variation in the footprints makes spectral comparisons for finding changes difficult.

MODIS data. For example, Hansen et al. (2008a) used the MODIS Vegetation Continuous Fields product to calibrate Landsat data to map forest disturbance in the Congo River Basin. Roy et al. (2008) developed a method for filling gaps in Landsat data using MODIS data. Gao et al. (2006) developed the Spatial and Temporal Adaptive Reflectance Fusion Model (STARFM) algorithm to predict Landsat surface reflectance using MODIS data. Hilker et al. (2009a,b) added a disturbance index based on the Tasseled Cap transformation to the STARFM algorithm to detect forest disturbance. In their work, two Landsat images acquired at the beginning and the end of a study period were used to delineate forest disturbances by thresholds in Tasseled Cap indices. A combination of Landsat and MODIS data was used to estimate the timing of disturbance at 8-day intervals using MODIS data. Their method yielded high accuracies but differs from the method presented here. Their approach essentially detected changes between pairs of Landsat images, and as such must wait for a new Landsat image to identify change. The method in this paper is intended to be used as close to near real-time as possible, by identifying forest disturbances on a daily basis as new MODIS swath data become available.

Here, we propose a fusion method different from the above-mentioned efforts in that we use Landsat data to predict MODIS observations. The overall benefit is to take advantage of the high temporal resolution of MODIS data to allow monitoring of forest disturbance in near real-time. The method is based on using a Landsat time-series to predict what new MODIS images should look like assuming the absence of forest disturbance or land cover change. The central hypothesis of the method is that our predicted MODIS images form a better baseline for comparison with actual MODIS observations than prior MODIS observations. Differences between predicted and observed MODIS images then become

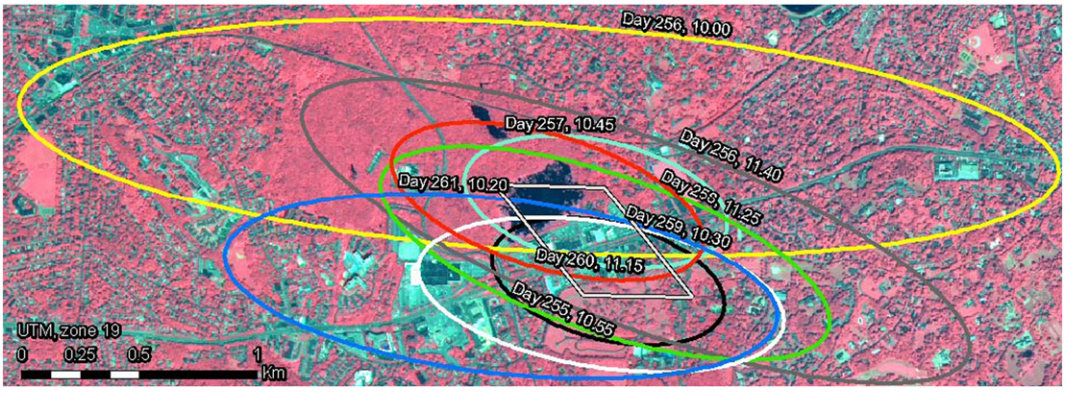

Fig. 1. The footprints of MODIS swath observations in a week overlaid on a QuickBird image. The observations shown are binned into the same 500 m grid cell (the white parallelogram). The footprints include the corresponding nominal area that contributes 75% of the signals and adjacent nominal area that contributes 25% of the signals.

indicative of forest disturbances. The first part of this paper describes the fusion method and the second part presents an application of the method for detecting forest clearing and thinning in an area in the Southeastern Unites States.

2. Study area and materials

We selected two study areas (Fig. 3) in the United States: one located in New England (NE) for evaluating the predicted images, and one located in the Savannah River Basin (SRB) on the border between the states of Georgia and South Carolina for evaluation of the ability to map forest disturbance. The study area of NE (Landsat Path 12 Row 31) exhibits a relatively low rate of forest disturbance (Jeon et al., 2012) and was chosen because significant surface change would complicate the evaluation of our efforts to predict what an image would look like in the absence of change. The SRB area (Landsat Path 17 Row 37) is characterized by intensive forest management and represents a challenging environment for finding forest disturbances at MODIS spatial resolution as most pixels are a mix of forest and agriculture or other land uses.

Temporally dense series of Landsat ETM + images (30 m spatial resolution; UTM projection) from the USGS open archive (WWW1) were used to predict MODIS daily images. All available ETM + images with a cloud cover less than 90% were downloaded (68 images 2000–2002 for the NE site, and 33 images 2001–2002 for the SRB site) for analysis.

Three kinds of standard MODIS products were used: the MODIS/Terra L2 swath surface reflectance product (MOD09), the MODIS/Terra L2G daily global gridded surface reflectance product (MOD09GA), and the MODIS L3 16-day global BRDF/albedo model parameter products (MCD43A1). All these products are available from NASA science data distribution centers (MOD09 from WWW2; MOD09GA and MCD43A1 from WWW3). MODIS data were acquired between September 11 to October 13 in 2000 for the NE study area and for the whole year of 2003 for the SRB study area. Details on these products can be found on the MODIS data website (WWW4).

To assess the accuracy and timeliness of the detection of forest disturbance using the fusion method, we need to know where and when disturbances occurred. Validation of multi-temporal detection of forest disturbance using the proposed method is challenging, because independent reference sources with well-recorded timing, acreage, and location of land change must be available for both ends of the change interval. A suitable source of reference data that meet these requirements is provided by temporally dense series of Landsat images. For this reason, we manually interpreted all available Landsat TM/ETM + images in a year to derive a reference map of forest disturbance for the SRB site (Fig. 4). The reference map thus represents the timeliest result that we can achieve using Landsat data.

A complete description of the production of the reference map is available in Zhu et al. (2012), and details provided here relate more directly to the fusion method. The reference map covers an area of 580 km^2 out of which 5% (29.4 km^2) is forest disturbance. The reference map consists of 21 rectangular areas for validation, each more than 3 × 3 km in size, where areas of forest disturbance were carefully identified. Based on the map of annual forest disturbances, interpreters sorted through all Landsat TM/ETM + images in 2003 (24 images with less than 90% cloud cover in total) to find the date when the forest disturbance had not yet occurred in 2003 (Fig. 4A) and when the disturbance could first be observed in Landsat data (Fig. 4B).

When trying to determine the date of disturbance for any day between Landsat acquisitions, there are three possibilities: (1) areas that have been disturbed during a prior time period – we refer to these areas as *known-date*; (2) areas that we know were disturbed during the time interval between acquisitions but we are not sure of the exact date – these are referred as *unsure-date*; and (3) areas that have not been disturbed, which are referred to as *undisturbed*. The detection of disturbance of *unsure-date* using the fusion approach would represent a timelier mapping of disturbance than is possible with Landsat.

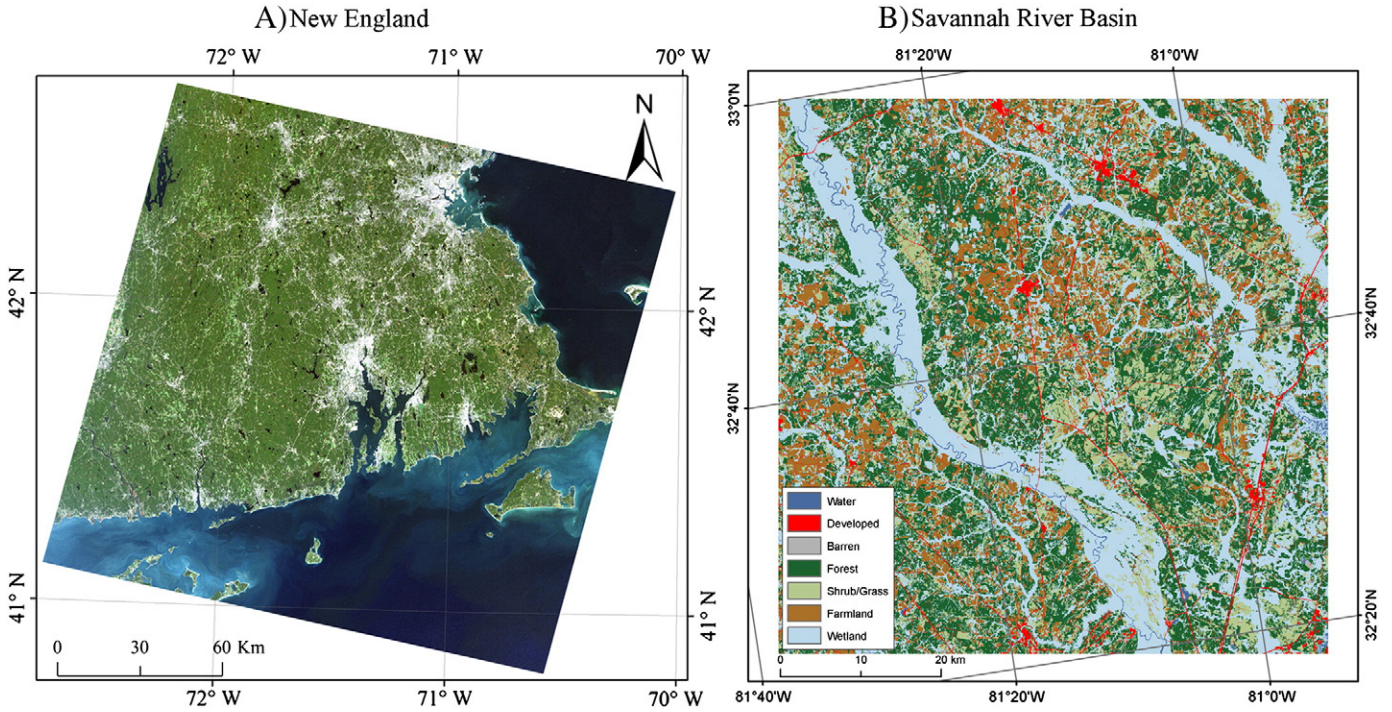

Fig. 3. The New England (NE) and Savannah River Basin (SRB) sites in United States. (A) A true-color composite image (Landsat Bands 3, 2, 1) showing the NE area. The Landsat image was collected on 27 Sep 2000. (B) A land cover map from the 2006 National Land Cover Data of the SRB site. Note that this is not the reference map of forest disturbance used for validation.

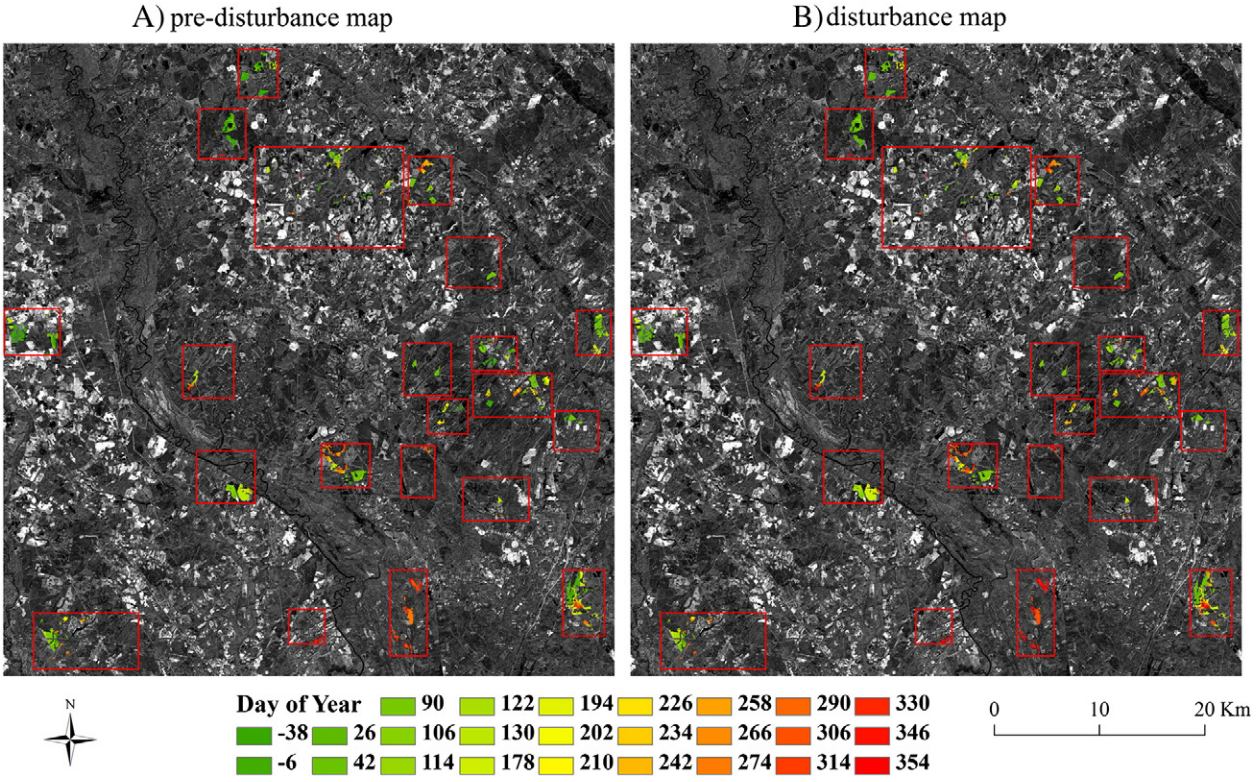

Fig. 4. The reference maps of forest disturbance at 30 m resolution. (A) This map shows the dates (represented by colors with negative values in 2002) that forest disturbances have not occurred in 2003 based on time-series images of Landsat TM and ETM+. (B) This map shows the dates (represented by colors) when forest disturbance in 2003 first could be identified in the Landsat time series. The backdrop is a 15 m Landsat ETM + panchromatic image collected on 23 Nov 2002.

3. Methodology

The workflow of our fusion system is presented schematically in Fig. 5. The fusion process consists of two major steps. The first step is to predict a Landsat image for a new date based on time-series analysis of Landsat data. The second step is to use the predicted Landsat image for a particular day to predict what the MODIS image should look like for that day. The prediction of MODIS swath observations from a finer resolution Landsat image is made possible by application of the MODIS Point Spread Function (PSF), and explicit consideration of the changing location and size of MODIS observations on a daily basis. To improve our efforts on predicting the next MODIS images, an additional step is made to correct the effects of viewing and illumination geometry. In this way, the predicted MODIS swath data can be compared with real MODIS acquisitions on the same day for monitoring forest disturbance.

3.1. Brief description of predicting daily Landsat data

A detailed description of this step is provided in Zhu et al. (2012) with a brief summary provided here, as it is fundamental to the presented methodology. First, a time series of Landsat ETM + images was atmospherically corrected and areas contaminated by cloud, cloud shadow and snow were masked out. A time series model was then fit for each pixel to predict daily surface reflectance. The time-series model used in this study is based on Fourier analysis that models the time-series as a function of sines and cosines (Zhu et al., 2012):

$$f(x) = a_0 + \sum_{i=1}^{N}\left(a_i \cos\left(\frac{2\pi}{iT}x\right) + b_i \sin\left(\frac{2\pi}{iT}x\right)\right) + a_{N+1}\cos\left(\frac{2\pi}{0.5T}x\right) + b_{N+1}\sin\left(\frac{2\pi}{0.5T}x\right) \quad (1)$$

where, x is the day of the year; N is the number of years; T is the number of days per year ($T = 365$); a_0 is the coefficient for overall surface reflectance; a_i and b_i are the coefficients that capture the changes for the ith year; and a_{N+1} and b_{N+1} are the coefficients that capture the bimodal change for each year.

This approach is computationally intensive since all parameters have to be successively fit for each of the six spectral bands of every Landsat pixel. The outliers, for example observations affected by clouds and cloud shadows, are removed during this process. Once the model is fit, it is possible to predict a Landsat image for any given day during or following the time-series. The model yielded R-square values above 0.9 between predicted and observed Landsat images (Zhu et al., 2012).

3.2. Predicting MODIS swath data from Landsat data

Efforts to use Landsat data to explore the anticipated characteristics of data at MODIS spatial resolutions predate the launch of MODIS (e.g. Barker & Burelhach, 1992; Moody & Woodcock, 1994). The MODIS Science Team developed general-purpose tools to aggregate Landsat data to MODIS spatial resolutions, including an effort to add sensor noise during the aggregation process. These programs, however, did not take into account the effects of view angles and the associated variability in the footprint of MODIS observations. In addition, there was no attempt to explicitly include the effects of Point Spread Function (PSF), which characterizes a sensor's response. Unlike Landsat, the MODIS PSF is modeled as triangular in the scan direction and square in the along-track direction, which means point sources on the ground surface do not contribute equally to a MODIS observation (Wolfe et al., 1998). Since the location, view angle and size of MODIS observations vary from day to day, our fusion method takes all these factors into account.

The fusion method simulates the acquisition process of MODIS by treating the predicted Landsat images as the ground surface, and

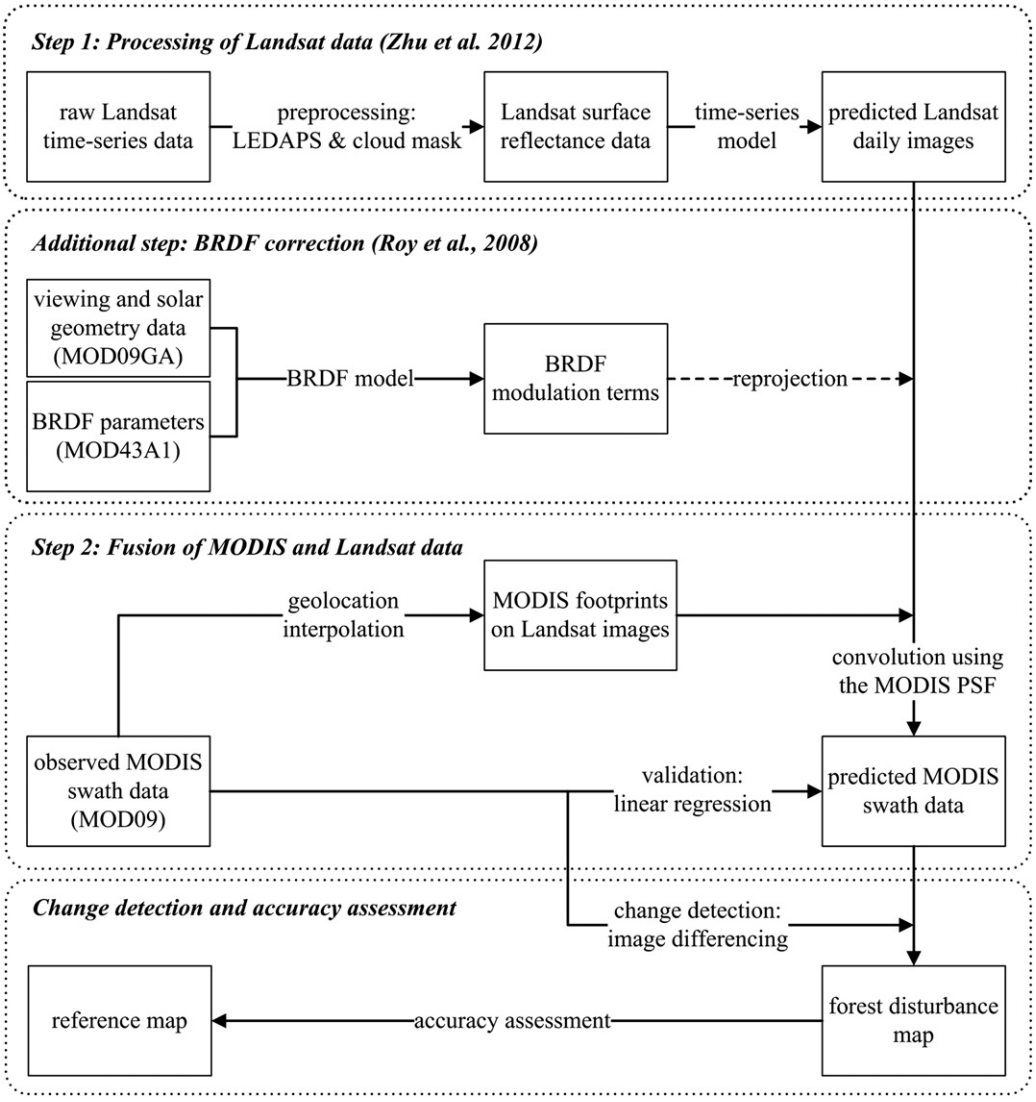

Fig. 5. The flowchart of the proposed methodology for detecting forest disturbance.

estimates MODIS swath data by carefully placing each MODIS footprint on the predicted Landsat images and convolving it with the sensor PSF.

A single observation of MODIS can be written as follows (Tan et al., 2006):

$$F_\lambda = \int_{y_0-\frac{\phi}{2}}^{y_0+\frac{\phi}{2}} \int_{x_0-\frac{\psi}{2}}^{x_0+\frac{\psi}{2}} w(x-x_0, y-y_0) f_\lambda(x,y)\,dx\,dy \quad (2)$$

$$w(x,y) = \begin{cases} \psi - |x-x_0| & (x,y) \in D \\ 0 & otherwise \end{cases} \quad (3)$$

where, F_λ is the electronic signal for wavelength λ collected by a MODIS observation centered at location x_0,y_0; f_λ denotes the spatial distribution of the reflectance from the ground surface, in this case, the Landsat surface reflectance data; x and y represent the locations of Landsat pixels with respect to the MODIS observation in the scan and along-track directions, respectively; ϕ and ψ are the dimensions of the MODIS observation in the scan and track directions, respectively; $w(x,y)$ is the MODIS PSF; and D is the footprint of the MODIS observation.

To solve the two equations above, accurate locations of the center and footprint of each MODIS swath observation are required. In other words, for every MODIS daily swath overpass, we have to locate the center position x_0 and y_0 of each MODIS swath pixel with respect to the Landsat images, orient the scan direction and along-track direction, and derive the pixel dimensions. This work is being done with MOD09 (the swath data) instead of MOD09GA (the daily gridded product), because some information, including the dimensions and centers of observations, is irretrievable after the MODIS gridding process.

The center locations of the 1 km MOD09 swath observations are given in latitude and longitude. These coordinates are transformed to UTM global coordinates to match the Landsat images. Interpolation is used to find the center locations for the 500 or 250 m pixels. This is done in two steps (Gumley et al., 2003): (1) in the along-track direction, each scan cycle of MODIS must be interpolated separately because of the overlap between successive scan cycles (Wolfe et al., 2002); (2) in the scan direction, it is required to offset the bilinear interpolation at different resolutions because the centers of 250, 500, and 1000 meter pixels of each scan cycle are co-registered (Nishihama et al., 1997). Fig. 6 shows the relative positions between the 1 km MODIS geolocation data and the derived 500 m centers.

In terms of orientation, the MODIS footprints at 250, 500 and 1000 m are considered to be in perfect alignment (Wolfe et al., 1998). The scan direction of each MODIS pixel is determined by the center locations of adjacent pixels along the scan line. The track direction is then perpendicular to the scan direction for each MODIS pixel.

The exact shape of a MODIS swath observation is possibly influenced by the atmosphere and topography. A rectangular shape is assumed by Tan et al. (2006). We have tested various shapes of the MODIS footprints, including oblong, rectangular, and oval. The oval shape gave the best results compared with real MODIS images, as measured by the coefficient of determination (R^2). Moreover, the oval shape is essentially the projection of a conical view from a point source. It fits the model of the triangular PSF in the scan direction and the square PSF in the track direction well. In fact, the shape of MODIS footprints were not found to have a strong impact on the simulations as the fine resolution pixels (i.e. Landsat data) within differences among those shapes have smaller PSF weights and contribute less to a MODIS swath observation than pixels in the center. Therefore, the oval shape (Fig. 6), including all areas that contribute to a MODIS observation, was adopted as a good approximation in our study.

Nominal dimensions of MODIS pixels in both the scan and along-track directions increase with increasing scan angles. The scan angles progressively increase from −55° to 55° with an increment of about 0.0406° for the 500 m pixels at a fixed altitude of 705 km. The MODIS products integrate ancillary data (e.g. digital elevation models) to calculate the altitude more precisely (Nishihama et al., 1997). At this stage, we have not compensated for the effects of topography, as the study areas are relatively flat. In future studies of mountainous terrain, we may need to consider topography effects to improve this simulation. As calculated based on functions defined in Appendix B of Tan et al. (2006), the dimensions of MODIS swath pixels are 2.4 km in the scan direction and 1.0 km in the track direction at the end of a scan line. These numbers are consistent with Wolfe et al. (1998).

With knowledge of individual MODIS footprints such as location, size and orientation (as shown in Fig. 6), the "predicted" MODIS spectral reflectance can be calculated by convolving the surface reflectance of all Landsat pixels according to the MODIS PSF. Since the predicted Landsat images are free of clouds, cloud shadows, and snow, this convolution process does not have to handle the cloudy or shadowed Landsat pixels. The minor differences in the spectral bands between Landsat and MODIS are ignored as in other fusion studies (e.g. Gao et al., 2006; Roy et al., 2008). Since our approach is based on predictions of a Landsat time-series, the difference in the overpass time between the Terra and Landsat platforms has little influence.

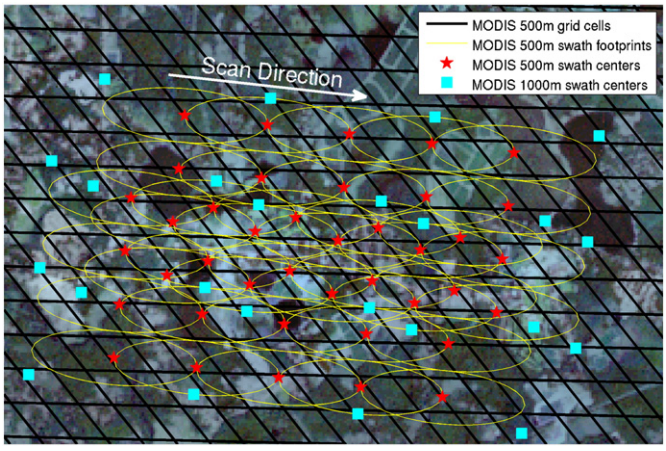

Fig. 6. The footprints of MODIS swath and gridded products overlaid on a Landsat ETM + image. The black lines are the boundaries of the MODIS grid cells and the yellow lines are the boundaries of the MODIS swath observations. The view zenith angles of MODIS swath observations are approximately 50°. The center points of the 500 m and 1 km swath observations data demonstrate their relative positions and illustrate the interpolation method.

3.3. BRDF correction

The Bidirectional Reflectance Distribution Function (BRDF) describes how the surface reflectance changes when viewed and illuminated from different angles. MODIS images are collected over a wide range of view angles, while predicted MODIS images based on Landsat images are essentially viewed from nadir. Therefore, it is important to account for the effects of bidirectional reflectance in predicted MODIS images. A simple solution based on the work of Roy et al. (2008) was tested to compensate for bidirectional reflectance effects.

The operational MODIS BRDF algorithm uses a linear BRDF model that relies on the weighted sum of an isotropic parameter and two kernels of viewing and illumination geometry (Schaaf et al., 2002):

$$R_{MODIS}\left(\Omega\Omega',\lambda_{MODIS}\right)=f_{iso}(\lambda_{MODIS})+f_{vol}(\lambda_{MODIS})\times k_{vol}\left(\Omega\Omega',\lambda_{MODIS}\right)+f_{geo}(\lambda_{MODIS})\times k_{geo}\left(\Omega\Omega',\lambda_{MODIS}\right) \quad (4)$$

where $R_{MODIS}(\Omega\Omega',\lambda_{MODIS})$ is the reflectance for the wavelength λ_{MODIS} with viewing vectors Ω and illumination vectors Ω'; $k_k(\Omega\Omega',\lambda_{MODIS})$ are the BRDF model kernels; and $f_k(\lambda_{MODIS})$ are the spectrally dependent BRDF parameters.

Roy et al. (2008) assumed that the MODIS modulation term c (defined below) for a particular MODIS wavelength λ_{MODIS} was representative of the reflectance variation at the Landsat scale for a spectrally similar Landsat ETM + wavelength λ_{ETM+}. The functions to correct the BRDF effects could then be described as:

$$c(\lambda)=\frac{R_{MODIS}\left(\Omega_{observed},\Omega'_{observed},\lambda_{MODIS}\right)}{R_{MODIS}\left(\Omega_{nadir},\Omega'_{observed},\lambda_{MODIS}\right)} \quad (5)$$

$$\hat{R}_{ETM+}(\lambda_{ETM+})=c(\lambda)\times R_{ETM+}(\lambda_{ETM+}) \quad (6)$$

where $R_{MODIS}\left(\Omega_{observed},\Omega'_{observed},\lambda_{MODIS}\right)$ is the surface reflectance of MODIS for the wavelength λ_{MODIS} sensed with viewing vectors $\Omega_{observed}$ and illumination vectors $\Omega'_{observed}$ for a given day; $R_{MODIS}\left(\Omega_{nadir},\Omega'_{observed},\lambda_{MODIS}\right)$ is the modeled reflectance with nadir viewing vectors Ω_{nadir} and illumination vectors $\Omega'_{observed}$; the modulation term $c(\lambda)$ is the ratio of off-nadir to nadir surface reflectance of MODIS for the wavelength λ; $R_{ETM+}(\lambda_{ETM+})$ is the surface reflectance from model fitting of a time series of Landsat ETM + images; and $\hat{R}_{ETM+}(\lambda_{ETM+})$ is the BRDF-adjusted Landsat reflectance.

Compensating for BRDF effects was done in three steps based on Eqs. (4) to (6). First, the BRDF Forward Model Tool (WWW4; Schaaf et al., 2002) was used to retrieve the surface reflectance of MODIS pixels for each spectral band. Inputs to the model include 16-day BRDF parameters (isotropic, volumetric, and geometric) obtained from the MCD43A1 product and daily viewing and illumination geometry data (resampled to 500 m) obtained from the MOD09GA product. The model generates MODIS surface reflectance data for specific viewing and illumination angles, including nadir. All inputs and outputs are gridded datasets at 500 m resolution in a Sinusoidal projection. Second, the modulation terms $c(\lambda)$ were calculated as the ratio of off-nadir to nadir surface reflectance for each band for each pixel, which were resampled to 30 m resolution (WGS-84/UTM) using the MODIS Reprojection Tool (WWW5). Third and last, the predicted Landsat daily surface reflectance data were multiplied by the modulation terms to correct for the bidirectional reflectance effects. In essence, predicted Landsat surface reflectance is corrected to the same viewing and illumination geometry as MODIS for a given day. Landsat data after BRDF correction are then convolved in the fusion process (described in Section 3.2) to predict MODIS swath data. In this way, the predicted and observed MODIS images for a given day have the same footprints and viewing and illumination geometry.

3.4. Evaluating predictions of MODIS data

An underlying hypothesis of the fusion method is that the predicted MODIS observations form a better baseline for comparison with actual MODIS observations than previously collected MODIS observations. To test this hypothesis, simple linear regressions were performed between predicted and observed MODIS images, and between successive days of actual MODIS images. A higher coefficient of determination (R^2) is considered a more robust baseline for comparison.

Such comparisons required screening the actual MODIS images for clouds, which was done by building cloud masks based on the ancillary MODIS quality data. Cloudy pixels were defined as observations with a cloud state, cloud shadow, cirrus detected, and internal cloud algorithm flags above zero in the quality metadata. To minimize the influence of clouds, we also tested a "buffer" algorithm, which labeled as cloudy all pixels within a distance of 3 pixels of a cloudy pixels in the MOD09 metadata. The MODIS surface reflectance product occasionally has negative reflectance because of the atmospheric correction, and a minimum threshold of 0.001 was used to remove negative values of surface reflectance. Comparisons of predicted MODIS images before and after BRDF correction were made separately to assess the impact of the BRDF correction approach.

3.5. Change detection using image differencing

There have been many kinds of algorithms proposed for change detection based on remotely sensed imagery (Coppin et al., 2004; Lu et al., 2004). At this stage, our primary concern is to test the fusion system to see if forest disturbances at the pixel or sub-pixel level of MODIS can be detected. For this reason, only image differencing, the most widely used change detection algorithm (Singh, 1989), was used to map forest disturbances.

To identify forest change, an empirical threshold of −0.070 for ΔNDVI was used in combination with a requirement that the MODIS pixels must be greater than 60% forest cover. The forest cover map was a by-product of the time-series analysis of Landsat imagery (Zhu et al., 2012). Tests were performed at both 250 m and 500 m resolution to determine how the spatial resolution influenced the ability of MODIS to detect changes, and to quantify the minimum size of disturbed patches that we could reliably detect. Even though the optimal threshold may vary with viewing geometry and spatial resolution, only one threshold was applied to detect forest disturbances for simplicity.

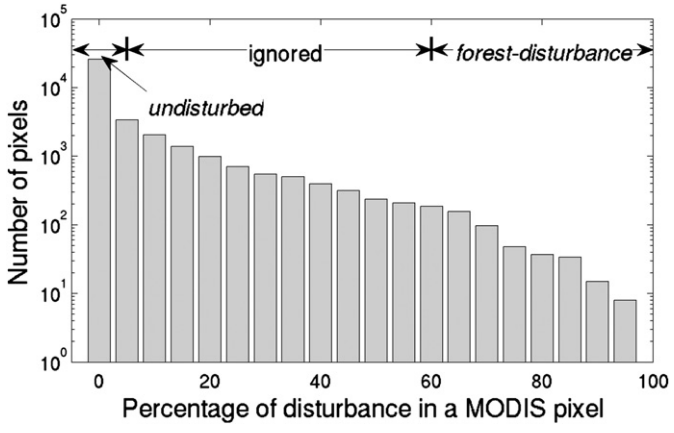

Fig. 7. The frequency distribution of forest disturbances in MODIS observations. The Y axis is logarithmic. This Figure illustrates the rule used in the accuracy assessment with a threshold 60%: (1) MODIS pixels with at least 60% disturbance must be mapped as *forest disturbance* to be considered correct; (2) pixels with less than 5% disturbance must be mapped as *undisturbed* to be considered correct, and (3) pixels with between 5 and 60% disturbance are left out of the accuracy assessment as it is unclear whether they should be considered in the *forest disturbance* or *undisturbed* class.

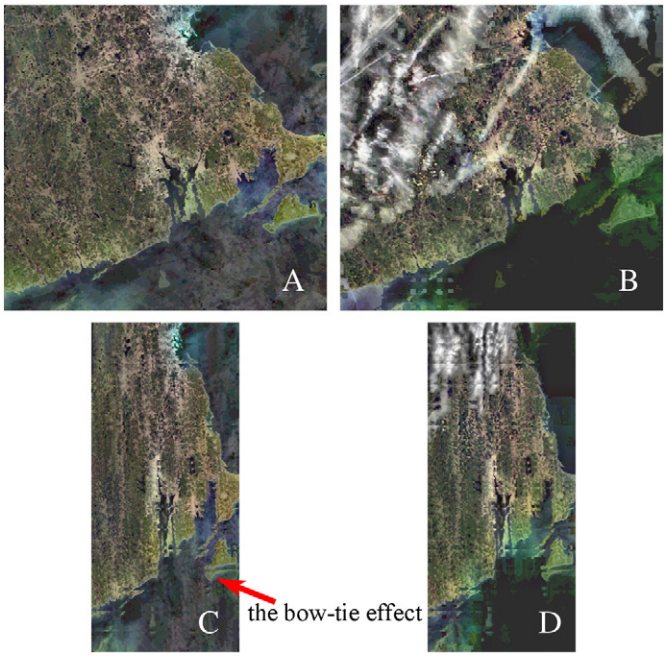

Fig. 8. Examples of predicted (left panel) and observed (right panel) MODIS swath images. (A) and (B) show predicted and observed true-color composites (MODIS bands 1, 4, 3) for the NE site at a view zenith angle of 4° (September 11, 2000). (C) and (D) are similar but MODIS observations were acquired at a view zenith angle of a 51° (September 17, 2000). Note that the predicted images are free of clouds even if it was cloudy on that day.

3.6. Accuracy assessment

Evaluating the pixel-level accuracy of change detection is complicated as we are evaluating a change map at a coarser resolution than the Landsat-based reference map. Usually, binary forest change maps have two distinct classes: *forest-disturbance* and *undisturbed*, and so does the subsequent accuracy analysis. However, in this study, there is a proportion of disturbance for each MODIS swath pixel. If no disturbance has occurred in the footprint of a MODIS observation, it is obvious that the observation should be labeled as *undisturbed*. Similarly, if 100% of a MODIS footprint has changed, it should be labeled as *forest-disturbance*. However, for the cases in-between, it is somewhat arbitrary to select a single threshold to separate the two classes.

Since our goal is to identify where forest disturbance is occurring, the smaller the percentage of disturbance that can be reliably found, the better. To address this question, we have defined the *forest-disturbance* class using five different proportions of disturbance: >60%, >50%, >40% >30% and >20% of a MODIS footprint (see an example in Fig. 7). For example, a disturbance proportion of >60% means that at least 60% of the MODIS footprint is disturbed according to the reference map. In this case, MODIS observations with a proportion greater than 60% disturbance are considered members of the *forest-disturbance* class, while observations with less than 5% disturbance are considered members of the *undisturbed* class. Observations with a disturbance proportion between 5% and 60% are ignored, as they cannot unambiguously be labeled either *forest-disturbance* or *undisturbed*. Thus, the *undisturbed* class in the reference map remains the same for different thresholds, while the *forest-disturbance* class grows as the thresholds decrease.

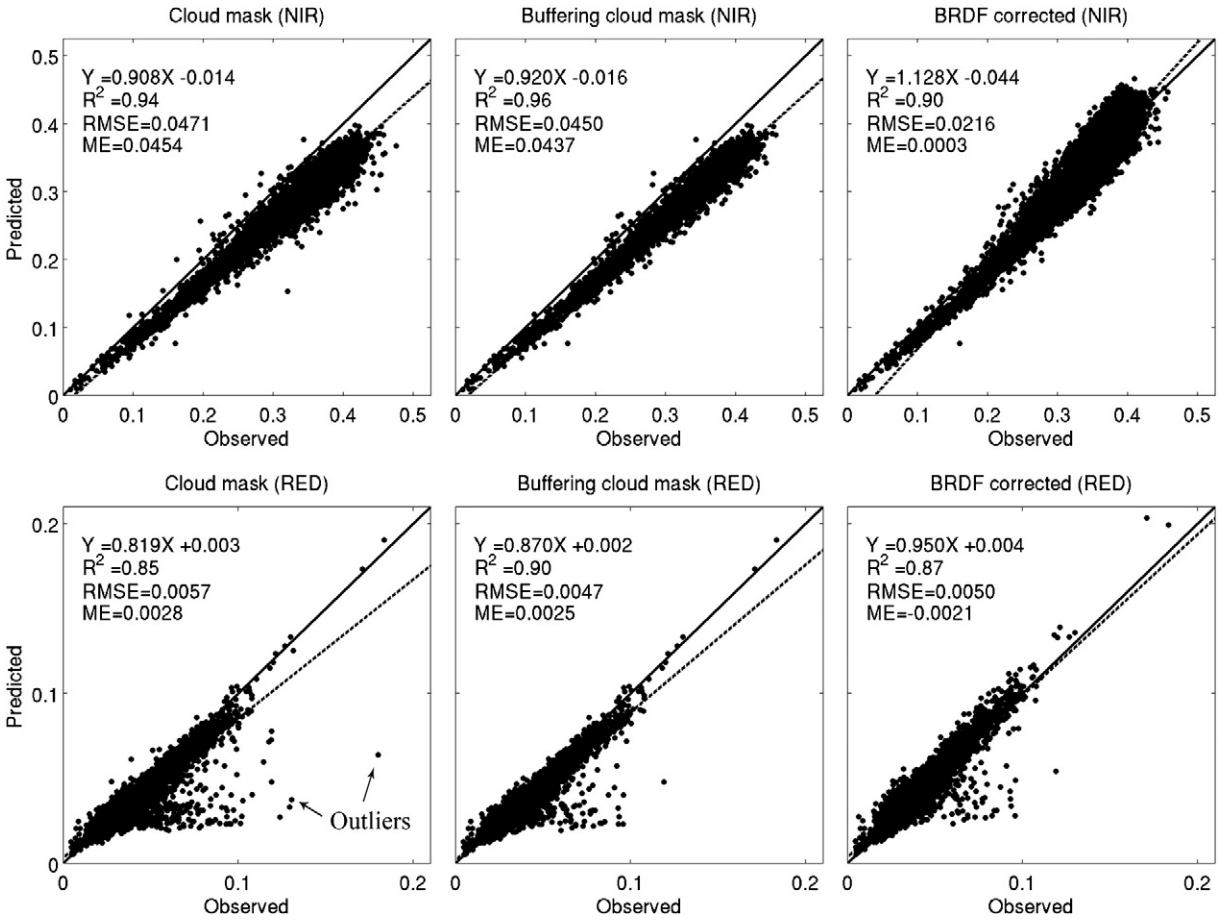

Fig. 9. Predicted versus observed surface reflectance. The spectral bands of NIR (top row) and red (bottom row) are compared for the off-nadir images (Fig. 8C and D) of the NE site. Comparisons were made for three cases: clouds screened using the MODIS cloud mask (left column); clouds screened using the MODIS cloud mask plus a 3-pixel buffer (middle column); BRDF correction plus cloud screened using the 3-pixel buffer (right column). The solid lines denote the 1:1 lines, and the dashed lines denote the regression lines.

To further complicate the issue, the disturbance polygons in the reference map are labeled either *known-date* or *unsure-date*. Consistent identification of *unsure-date* could demonstrate the advantage of timelier detection using the fusion method than using Landsat data alone, but these pixels are excluded since we cannot be sure of the exact date when the changes occurred. For this reason, although the forest disturbance maps contain changes throughout 2003, we only validate results from the last four months (September 1 to December 31, 2003) to minimize the influence from the *unsure-date* class.

For quantitative evaluation, the primary metrics for accuracy used in this paper are the producer's, user's, and overall accuracy. These are typically probabilistic measures of map accuracy estimated from a probability sample (Olofsson et al., 2013). In this case, our reference maps do not constitute a probability sample and these measures should therefore not be interpreted as probabilistic measures of map accuracy but as measures of the amount of omission, commission and overall error in the generated disturbance maps. High producer's accuracy means less omission error, while high user's accuracy implies less commission error. In this study, producer's, user's and overall accuracies are defined as:

$$\text{Producer's Accuracy} = \frac{\text{Number of pixels with } \textit{"known-date"} \text{ correctly identified}}{\text{Number of pixels with } \textit{"known-date"} \text{ in reference maps}} \quad (7)$$

$$\text{User's Accuracy} = \frac{\text{Number of pixels with } \textit{"known-date"} \text{ correctly identified}}{\text{Number of pixels identified as disturbances in produced maps}} \quad (8)$$

$$\text{Overall Accuracy} = \frac{\text{Number of pixels correctly identified}}{\text{Number of all pixels}} \quad (9)$$

Another metric is the site-level detection rate, which measures how often and consistently individual patches of disturbance can be detected. For this analysis, a number of individual patches are identified, and the detection rate describes the frequency with which they are detected. Note that the detection rate is unrelated to errors of commission and benefits from a low threshold. It therefore needs to be interpreted together with the proportion of commission errors (i.e. the user's accuracy).

$$\text{Detection Rate} = \frac{\text{Number of days with patches detected}}{\text{Number of days with cloud} - \text{free observations}} \quad (10)$$

4. Results

4.1. Prediction of MODIS observations

True-color composite images of both near-nadir (Fig. 8A and B) and off-nadir (Fig. 8C and D) "predicted" and observed MODIS swath data at 500 m resolution are shown in Fig. 8. The predicted images are always free of clouds even if it was cloudy on that day. The phenomenon of pixel duplication due to the "bow-tie" effect (Wolfe et al., 1998), whereby successive MODIS scans overlap each other at the edge of a swath, can be seen in both the predicted and the observed swath data. This phenomenon is more pronounced for observations collected off-nadir (Fig. 8C and D). In addition, the

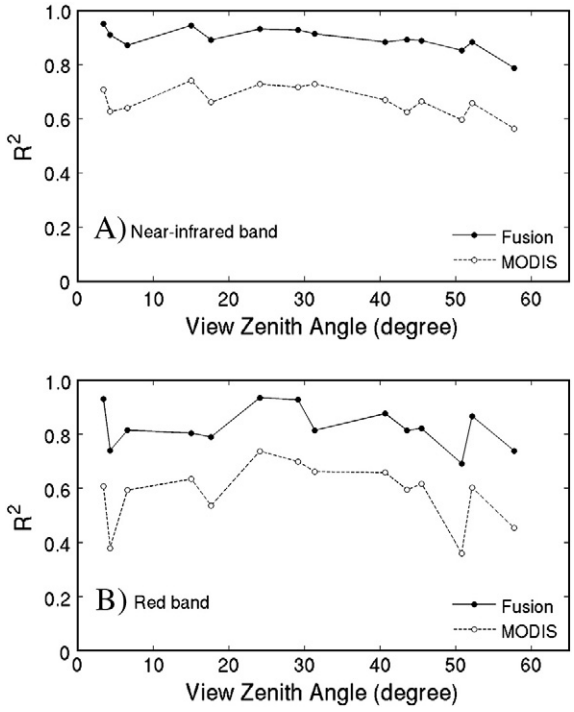

Fig. 10. The coefficients of determination (R^2) between predicted and observed MODIS images (denoted by "Fusion"), and between a MODIS image acquired at nadir and MODIS images on successive days (denoted by "MODIS") for the NE site. Values of surface reflectance in both the red (Fig. 10A) and NIR (Fig. 10B) bands are compared for cloud-free MODIS observations between September 11 and October 13, 2000. MODIS images acquired at different view zenith angles are corrected to nadir viewing based on the method described in Section 3.3.

blurring effect of large view angles and the reduced number of swath pixels that are necessary to cover the same area are apparent when comparing near nadir with off-nadir images.

Quantitative comparisons of the predicted and observed MODIS off-nadir images (i.e. Fig. 8C and D) are illustrated in Fig. 9. Correlations were found to be high for cloud-free pixels with the R^2 values of 0.94 for the NIR band, and 0.85 for the red band. The lower R^2 values in the red band are probably due to stronger atmospheric scattering in the red band than in the NIR band. Some values deviate from the 1:1 line, particularly for the red band (left column in Fig. 9). Close examination of these outliers reveals that many of them are in close proximity to pixels flagged as clouds in the MODIS metadata. Many of these outliers are removed when using the 3 pixel buffering approach (middle column in Fig. 9). The outliers are likely pixels partially covered with clouds, as the observed reflectance is generally anomalously high.

The high R^2-values between observed and predicted MODIS off-nadir images (51° view zenith angle) demonstrate that we have successfully modeled the primary components of the MODIS sensing process. However, due to the limited range of view angles in the Landsat data, our predictions of MODIS data are essentially for near-nadir view. As a result, the BRDF effects of the land surface undermine the relationship as the viewing and solar geometry of MODIS observations vary every day. For example, the predicted values of surface reflectance are biased as indicated by a large mean error of 0.044 in the NIR band (middle column in Fig. 9). In comparison, the BRDF correction approach can effectively shift the predicted surface reflectance closer to the 1:1 line (right column in Fig. 9). Note that this BRDF correction approach is far from perfect as we are assuming that all 30 m pixels within a 500 m MODIS grid cell have the same BRDF correction factor.

Fig. 10 further demonstrates the advantage of our fusion method in terms of providing a better basis for comparison with real MODIS images than the use of prior MODIS images. It shows the R^2 values between predicted and observed MODIS observations, and between a nadir-viewing MODIS image (September 27, 2000) and MODIS images on successive days. BRDF correction was performed for MODIS images acquired at different angles using a similar approach as described in Section 3.3. The pattern from the fusion method for one day (shown in Fig. 9) is repeated for the others: higher R^2 values for the NIR than the red band, and the R^2 values routinely above 0.85 in the NIR and 0.75 in the red bands. In comparison, the R^2 values between successive days of BRDF-corrected MODIS images are significantly lower. They range from about 0.65 to 0.75 in the NIR and vary widely in the red band, averaging less than 0.6. Similar to the comparisons with the predicted MODIS images, the R^2 values for the NIR band are higher than for the red band, probably due to the atmospheric effects. It is important to remember that these comparisons of MODIS data are against a nadir image, and the size of MODIS footprints changes as the view angle increases. In some regard, the results of the comparisons of MODIS observations near nadir represent the best-case scenario, and despite being surprisingly low, the observed R^2 values are at the high end of results we have found in other tests, e.g. using an off-nadir MODIS reference or comparing successive days of MODIS images without BRDF correction.

4.2. Detection of forest disturbance in the Savannah River Basin

The fusion method was applied in the Savannah River Basin (SRB) to detect forest disturbance. For better visualization, the daily maps of forest disturbance at MODIS scale were reprojected to UTM projection and areas flagged as *disturbed* draped on top of a Landsat image (Fig. 11).

For a more detailed visual inspection of the result, an enlargement of the cyan rectangle in Fig. 11 is displayed in Fig. 12. Results from NDVI differencing are shown for five different days at 500 m and 250 m resolution. The red and cyan patches in Fig. 12 represent areas of *known-date* (i.e. we know the disturbance date) and *unsure-date* (i.e. we are not sure on the disturbance date), respectively. Yellow lines denote the boundary of the MODIS footprints flagged as *disturbed* by differencing predicted and observed NDVI. Note that all areas of disturbance have been mapped without errors on December 28 at 250 m spatial resolution (Fig. 12j).

A relevant question is whether the fusion method can detect changes earlier than using only Landsat data. As shown in Fig. 12, polygon (A) flagged on October 16 by the fusion method is detectable from the Landsat time series on November 2. The fusion method identified this disturbance 17 days before the first possible detection using Landsat images. Similarly, polygon (B) is detected by Landsat on December 20, while the fusion method flags the disturbance on December 7 (13 days earlier). The fusion method thus provides a more precise estimate of the time of a disturbance event, which is made possible by the higher temporal resolution of MODIS. Between September and December in 2003, there are only 6 non-cloudy Landsat images available but 45 Terra/MODIS acquisitions with less than 90% cloud cover, including 15 images with a view zenith angle less than 35°. Given the frequent cloud cover during the growing season in this area, the fusion method has clear advantages for detecting disturbances earlier than using Landsat data alone.

Which disturbances are detected is partially dependent on the view zenith angles and the footprints of the observations on that day. For example, in the 500 m disturbance maps, the bottom half of polygon (A) in Fig. 12b is missed due to increasing observation sizes. Although the disturbance maps shown in Figs. 12c and 12d have similar view angles and observation dimensions, the lower part of polygon (A) goes undetected due to the varying centers and orientations of the MODIS swath observations. The 250 m disturbance maps (Figs. 12f-j) better match the shape of the reference polygons and detect smaller changes (e.g. polygon D in Fig. 12j) simply because of the finer resolution.

In addition, errors of commission are present in the disturbance maps generated at both resolutions (Fig. 12c and e; and h and i).

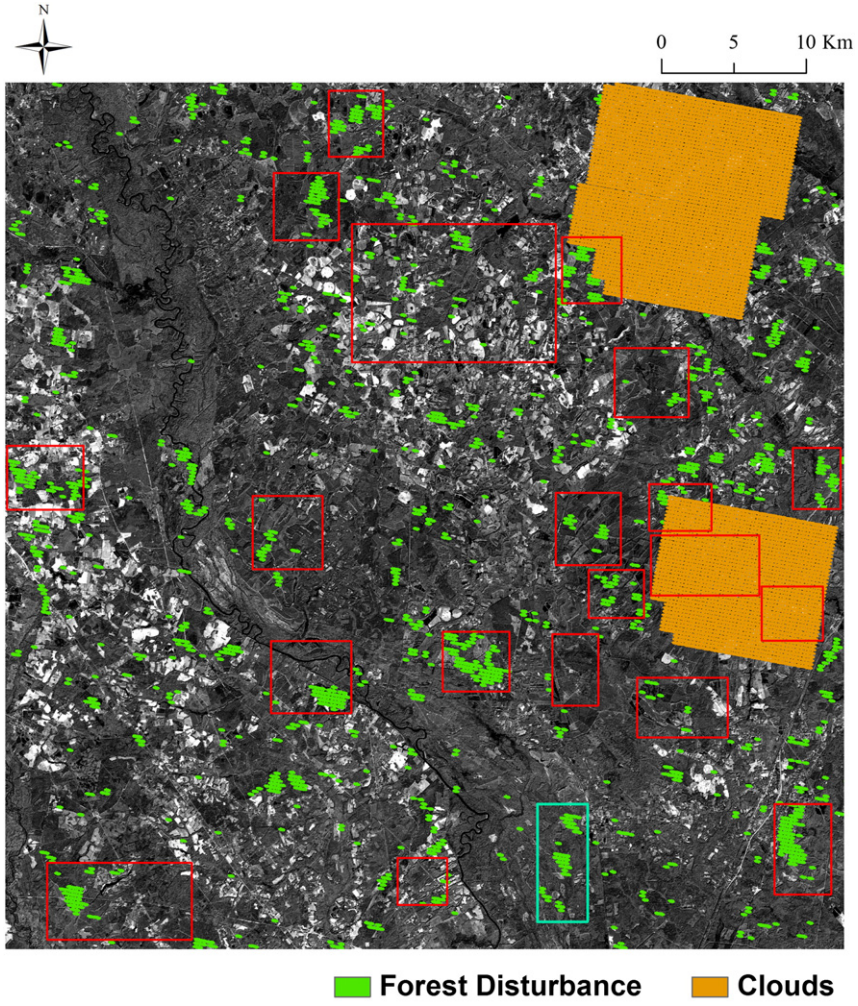

Fig. 11. A 30 m map of forest disturbance produced by the fusion method for December 28, 2003. For better visualization, disturbance maps at MODIS scale were reprojected to 30 m to match Landsat data. The backdrop is a 15 m Landsat ETM + panchromatic image collected on November 23, 2002. The cyan rectangular is shown in Fig. 12.

These footprints cover an area (polygon C in Fig. 12c) that was identified as forest thinning in the previous year (late 2002), possibly contributing to the confusion in this location.

4.3. Accuracy assessment of the change detection results

The error matrix in Table 1 shows high producer's and user's accuracy for the *forest-disturbance* class at 250 m resolution. The fusion method is able to detect >40% subpixel *forest-disturbance* with a producer's accuracy of 81% and a user's accuracy of 90%. The accuracies for *undisturbed* class and the overall accuracy are above 95%.

It is worth noting that the producer's accuracies decrease from 92% to 62% while the user's accuracies increase from 83% to 92% as the definition of *forest-disturbance* decrease from >60% to >20% (Table 1). The reasons are as follows: as the definition of *forest-disturbance* decreases, the number of disturbed pixels with a relatively subtle difference in reflectance between observed and predicted image will increase, which result in larger omission errors and thus lower producer's accuracy. On the other hand, the number of *undisturbed* pixels remains the same for all thresholds while the number of pixels correctly flagged as *forest-disturbance* will increase. Thus, the percentage of commission errors will decrease resulting in a higher user's accuracy. For these reasons, the producer's accuracy of 92% for >60% subpixel disturbance (Table 1) indicates that large patches of *forest-disturbance* are detected with low omission errors, and the user's accuracy of 92% for >20% subpixel disturbance indicates a low level of errors of commission.

Given low errors of commission, the detection rate shown in Table 2 demonstrates that disturbed patches down to about 5–7 ha are consistently detected in this study area. The minimum detectable patch of forest disturbance was investigated by examining the detection rates for 27 patches of forest disturbance. The patches examined varied in size with 18 patches being between 5 and 10 ha. The detection rate is high (at least 80%) for patches larger than 7 ha and becomes more inconsistent for patches smaller than 5 ha. In addition to assessing the daily detection rate, the rate was examined for maps composited over 16 days. A patch of *forest disturbance* was considered detected if it was flagged by any of the disturbance maps over a 16-day period. The detection rates for the composites are higher than the daily detection rates for all examined patches (Table 2).

5. Discussion

5.1. Minimum detectable patch size

When assessing the performance of a change detection method, the minimum detectable patch size is an important measure. Setting a general requirement for the minimum detectable patch size is difficult as the nature and scale of forest disturbance may vary considerably.

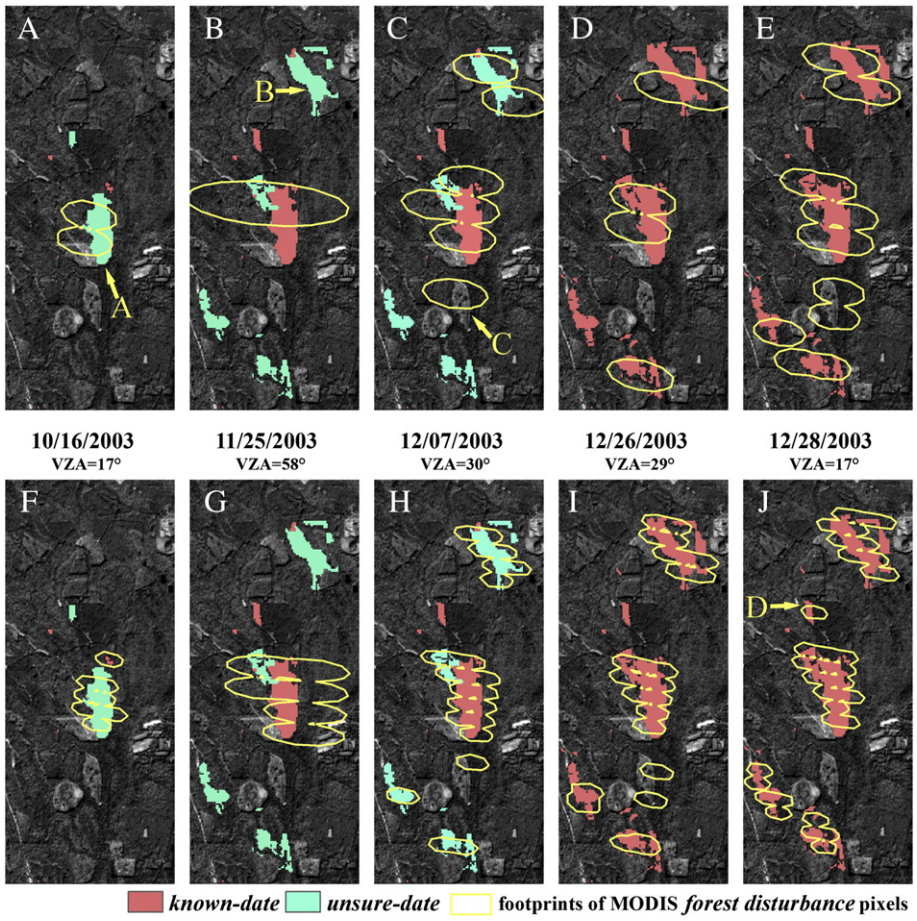

Fig. 12. Close-up of the cyan rectangle in Fig. 11. Results at both 500 m (top panel) and 250 m (bottom panel) are presented for five days with different view zenith angles. The yellow lines show the footprints of MODIS swath pixels flagged as forest disturbance.

Due to the coarse spatial resolution and varying footprints of MODIS data, per-pixel characterization of forest disturbance is challenging. Minimum detectable patch sizes reported in other MODIS-based change detection systems (e.g. Bucha & Stibig, 2008; Ferreira et al., 2007; Shimabukuro et al., 2006) are usually in the range of 15–50 ha (i.e. several 250 m pixels) although the average patch size of forest disturbance is typically less than 10 ha (Table 3). In other words, even if accurate, a change detection system operating at minimum scales of 15–50 ha may inherently underestimate the amount of human-induced forest disturbances. For example, the average size of disturbed patches in this study is 5 ha with only 3% of the patches larger than 25 ha. With a minimum detectable patch size of 25 ha, 97% of the forest disturbance would go unnoticed.

A change detection system based on daily image acquisitions that could detect disturbance MODIS pixel or subpixel level would contribute significantly to the monitoring of forest disturbance. With the methodology presented in this paper, per-pixel detection of forest disturbance based on MODIS data is possible as pairs of predicted and observed images are matched precisely in terms of footprints and sensor responses. However, the rather limited set of

Table 1
Error matrix generated by cross-tabulating reference and disturbance maps (NDVI, 250 m resolution). The matrix shows the number of pixels in the disturbance maps correctly flagged as *undisturbed* and *forest disturbance* (FD) for varying proportions of MODIS subpixel disturbance.

	Reference maps					Undisturbed	User's [%]
	FD > 60%	FD > 50%	FD > 40%	FD > 30%	FD > 20%		
FD	3976					789	83
Undisturbed	337					134,615	
FD		5440				789	87
Undisturbed		805				134,615	
FD			6962			789	90
Undisturbed			1603			134,615	
FD				8389		789	91
Undisturbed				3121		134,615	
FD					9539	789	92
Undisturbed					5863	134,615	
Producer's [%]	92	87	81	73	62		
Overall [%]	99	99	98	97	96		

Table 2
The detection rate at the polygon level for a number of patches of forest disturbance ranging from 2.1 to 113 ha in size. Forest disturbance maps were produced by image differencing of NDVI. The analysis includes cloud-free MODIS pixels from September to December in 2003. Bolded and underlined results are patches that can be detected with high rates (> = 80%) on a daily basis.

Patch size [ha]	Detection rate (%)	
	Daily	16-day composite
113	**100**	**100**
18.8	**100**	**100**
14.4	**100**	**100**
11.1	**80**	**100**
9.2	**93**	**100**
8.8	**87**	**100**
8.3	**100**	**100**
7.7	**87**	**100**
7.5	**87**	**100**
7.3	**93**	**100**
7.3	**80**	**100**
7.1	**93**	**100**
7.1	**80**	**100**
6.9	63	80
6.6	**87**	**100**
6.2	**93**	**100**
6.0	**92**	**100**
5.8	50	83
5.6	47	86
5.3	**93**	**100**
5.1	53	86
4.9	**81**	**83**
4.2	7	17
3.1	**90**	**100**
3.0	27	33
2.8	0	17
2.1	55	83

patches (27 in total) is insufficient for determining a final detectable minimum patch size. The investigation is also confined to only one location (the Savannah River Basin) further reducing the robustness of the results. A more thorough accuracy assessment involving more samples, preferably across larger areas, is needed to determine the smallest area of disturbance detectable.

5.2. Near real-time monitoring

The presented methodology is capable of monitoring forest disturbance in near real-time. Required inputs for making predictions of MODIS data were obtained from Landsat data in previous years (2001–2002), and forest disturbance was mapped by comparison to daily MODIS data in the subsequent year (2003). In essence, a disturbance map can be produced as soon as a new MODIS image is acquired.

A system monitoring forest disturbance at high spatial and temporal resolution would provide valuable information for managing and protecting forests. For example, ongoing projects in Brazil (INPE, 2002) attempt to identify areas 25 ha or larger of forest disturbance in the Amazon Basin every 2 weeks based on MODIS data. If the proposed method can detect disturbance less than 10 ha, it would offer a valuable contribution to such projects.

Table 3
The average patch size of forest disturbance for a few locations, as reported in the literature.

Places	Patch size (ha)	Sources
Romania	7.9	Olofsson et al. (2011)
Ukraine	4.8–9.3	Kuemmerle et al. (2007)
Slovakia	3.0–5.7	Kuemmerle et al. (2007)
Poland	1.7–4.0	Kuemmerle et al. (2007)
Rondônia, Brazil	<5	Ferraz et al. (2005)
Savannah River Basin, U.S.	5	This study

Another question concerns how frequently we need observations to identify forest disturbances with confidence. A forest disturbance is persistent, such that if a patch of disturbance is detected in several successive days the probability of it actually being forest disturbance is likely to increase significantly (Pouliot et al., 2009). The results in Table 2 also show higher detection rate based on 16-day composites than based on daily data. Therefore, one direction for future research will be how to integrate the results over successive days to improve the change detection and minimize errors. One possible solution is to provide a “possible change” flag the first time a disturbance is detected and a “confident change” designation after consistent detections.

5.3. Future improvements

In this study, careful consideration has been made to match the predicted and observed MODIS daily images precisely. Subsequent change detection has shown to work well even with a basic algorithm of image differencing. Still, the fusion method needs refinements, and its performance could be further improved.

First, predicting Landsat images for any given day is critical as it forms the basis for predicting daily MODIS images. Accurate prediction is dependent on the availability of Landsat images, which is of concern outside the United States (Kovalskyy & Roy, 2013). For many parts of the world, few or none Landsat images from the 1990s are available in the USGS Landsat archive. Since the implementation of the Landsat-based prediction model requires twelve clear Landsat observations to make a prediction (Zhu et al., 2012) and since we are comparing predictions to MODIS observations, which are available from 2000, this is less of an issue. However, cloud cover in the humid tropics and snow cover at high latitudes are likely to reduce the availability of useful Landsat images.

Second, improving the correction for bi-directional reflectance effects is likely to enhance the performance of the methodology. We have tested an automated correction approach based on MODIS standard products and integrating the quality control data in the MODIS BRDF product (MCD43A1) may be necessary in future tests (Roy et al., 2008). In addition, this approach is far from perfect as we are assuming that all 30 m pixels within a MODIS grid cell have the same BRDF correction factor. Future improvement should include exploration of other correction approaches. One approach is to use a land cover map at fine resolution, and apply different BRDFs for each land cover type, following the efforts of MODIS albedo validation (Liang et al., 2002; Roman et al., 2010).

Third, the method used to infer changes between predicted and observed observations influences the accuracy strongly. Only the most basic method of image differencing was tested. The thresholds were determined empirically for a relatively small area, and applying these over large areas could be problematic. Since more advanced methods have been applied for change detection based on remotely sensed images (Lu et al., 2004), further testing of other methods is necessary as robust non-empirical methods are preferable for large-scale applications.

Fourth, many of the commission errors identified in the accuracy assessment were in locations where the forest disturbance occurred prior to the study period. Since the predicted time-series was based on one year of observations prior to the study period, the time-series model incorrectly identifies these areas as intact forest, which results in commission errors when the predictions are compared to actual observations. The new implementation of the Landsat-based prediction model does not need a full year of data but twelve clear observations to initiate the prediction (Zhu et al., 2012). Future versions of the fusion method will make use of this updated algorithm, which is likely to decrease the number of commission errors.

Finally, this method needs to be evaluated in other locations. This would allow for a better evaluation in terms of minimum detectable patch size and near real-time performance. Hotspot areas

of deforestation and forest degradation such as the Amazon Basin, Congo Basin, and Southeast Asia would be suitable locations for further evaluation.

6. Conclusions

In this study, we present a novel approach for near real-time monitoring of forest disturbance using a combination of MODIS and Landsat data. Fusion of Landsat and MODIS data shows promise for providing a more robust baseline for comparison with new MODIS images than using previously collected MODIS images. Correlations between predicted and observed MODIS images were found to be high with R^2 values routinely above 0.85 for the NIR band and 0.75 for the red band. Comparing gridded MODIS BRDF-corrected observations at nadir and on consecutive days only yields the R^2 values in the range of 0.65–0.8 in the NIR band and about 0.5 in the red band. As a result, the presented methodology was able to detect 40% subpixel disturbance with a producer's accuracy of 81% and a user's accuracy of 90%. Although limited, accuracy assessment at polygon-level suggested that patches of forest disturbance down to about 5 to 7 ha could be detected consistently.

Our work also demonstrates the importance of view angle effects of MODIS data. The footprints and the center points of MODIS swath observations vary considerably from day to day, and the spectral signatures in the same grid cell are inherently different from each other. This problem undermines the use of MODIS daily products for change detection. The fusion method circumvents this problem as the varying MODIS footprints are explicitly handled, such that pairs of predicted and observed MODIS images are matched precisely.

The nature of this study is a pathfinder toward providing a stand-alone product that monitors forest disturbance globally in near real-time. Such products would be of great importance to protect forested areas efficiently and ensure the sustainability of our Earth system. When more Landsat-like satellite systems (e.g. Landsat Data Continuity Mission, Sentinel 2) become available, monitoring of forest disturbance in near real-time will be made easier as the frequency of observations will increase. In the meantime, the proposed method of fusion of currently available MODIS and Landsat data, though computational, shows the potential in the domain of near real-time monitoring of forest disturbance.

Acknowledgments

We thank Friedl, M.A. and Myneni, R.B. at Boston University and Schaaf, C. at University of Massachusetts for helpful comments on the manuscript. We also thank Wang, Z. at University of Massachusetts for helping data preparation and process.

References

Barker, J. L., & Burelhach, J. W. (1992). MODIS image simulation from Landsat TM imagery. *ASPRS/ACSM/RT, 92* (pp. 156–165). Bethesda, Washington, DC: American Society for Photogrammetry and Remote Sensing.

Bucha, T., & Stibig, H. (2008). Analysis of MODIS imagery for detection of clear cuts in the boreal forest in north-west Russia. *Remote Sensing of Environment*, *112*, 2416–2429.

Carroll, M. L., DiMiceli, C. M., Townshend, J. R. G., Sohlberg, R. A., Hansen, M. C., & DeFries, R. S. (2004). *Vegetative cover conversion MOD44A, burned vegetation, collection 4.* College Park, Maryland: University of Maryland.

Coppin, P., Jonckheere, I., Nackaerts, K., Muys, B., & Lambin, E. (2004). Digital change detection methods in ecosystem monitoring: A review. *International Journal of Remote Sensing*, *25*, 1565–1596.

DeFries, R. S., Field, C. B., Fung, I., Collatz, G. J., & Bounoua, L. (1999). Combining satellite data and biogeochemical models to estimate global effects of human-induced land cover change on carbon emissions and primary productivity. *Global Biogeochemical Cycles*, *13*(3), 803–815.

Ferraz, S. F. D., Vettorazzi, C. A., Theobald, D. M., & Ballester, M. V. R. (2005). Landscape dynamics of Amazonian deforestation between 1984 and 2002 in central Rondonia, Brazil: Assessment and future scenarios. *Forest Ecology and Management*, *204*, 67–83.

Ferreira, N. C., Ferreira, L. G., Huete, A. R., & Ferreira, M. E. (2007). An operational deforestation mapping system using MODIS data and spatial context analysis. *International Journal of Remote Sensing*, *28*(1), 47–62.

Gao, F., Masek, J., Schwaller, M., & Hall, F. (2006). On the blending of the Landsat and MODIS surface reflectance: Predicting daily Landsat surface reflectance. *IEEE Transactions on Geoscience and Remote Sensing*, *44*, 2207–2218.

Gong, P., & Xu, B. (2003). Remote sensing of forests over time: Change types, methods, and opportunities. In M. A. Wulder, & S. E. Franklin (Eds.), Massachusetts: Kluwer Academic Publishers.

Gumley, L., Descloitres, J., & Schmaltz, J. (2003). Creating Reprojected True Color MODIS Images: A Tutorial. Available at: http://earthdata.nasa.gov/library/creating-reprojected-true-color-modis-images-tutorial (accessed on 20 July 2012)

Hansen, M. C., Roy, D. P., Lindquist, E., Adusei, B., Justice, C. O., & Altstatt, A. (2008a). A method for integrating MODIS and Landsat data for systematic monitoring of forest cover and change in the Congo Basin. *Remote Sensing of Environment*, *112*, 2495–2513.

Hansen, M. C., Stehman, S. V., Potapov, P. V., Loveland, T. R., Townshend, J. R. G., DeFries, R. S., et al. (2008b). Humid tropical forest clearing from 2000 to 2005 quantified by using multitemporal and multiresolution remotely sensed data. *Proceedings of the National Academy of Sciences of the United States of America*, *105*, 9439–9444.

Hilker, T., Wulder, M. A., Coops, N. C., Linke, J., McDermid, G., Masek, J. G., et al. (2009a). A new data fusion model for high spatial- and temporal-resolution mapping of forest disturbance based on Landsat and MODIS. *Remote Sensing of Environment*, *113*, 1613–1627.

Hilker, T., Wulder, M. A., Coops, N. C., Seitz, N., White, J. C., Gao, F., et al. (2009b). Generation of dense time series synthetic Landsat data through data blending with MODIS using a spatial and temporal adaptive reflectance fusion model. *Remote Sensing of Environment*, *113*, 1988–1999.

Huang, C. Q., Townshend, J. R. G., Liang, S., Kalluri, S. N. V., & DeFries, R. S. (2002). Impact of sensor's point spread function on land cover characterization: Assessment and deconvolution. *Remote Sensing of Environment*, *80*, 203–212.

Instituto Nacional de Pesquisas Espaciais (INPE) (2002). *Deforestation estimates in the Brazilian Amazon.* Brasilia: São José dos Campos, Minist. da Ciênc.e Tecnol (Available at http://www.obt.inpe.br/prodes/)

Jeon, S. B., Olofsson, P., & Woodcock, C. E. (2012). Land use change in New England: A reversal of the forest transition. *Journal of Land Use Science*, 1–26. http://dx.doi.org/10.1080/1747423X.2012.754962.

Jin, S. M., & Sader, S. A. (2005). MODIS time-series imagery for forest disturbance detection and quantification of patch size effects. *Remote Sensing of Environment*, *99*, 462–470.

Kennedy, R. E., Yang, Z., & Cohen, W. B. (2010). Detecting trends in forest disturbance and recovery using yearly Landsat time series: 1. LandTrendr — Temporal segmentation algorithms. *Remote Sensing of Environment*, *114*, 2897–2910.

Kovalskyy, V., & Roy, D. P. (2013). The global availability of Landsat 5 TM and Landsat 7 ETM + land surface observations and implications for global 30 m Landsat data product generation. *Remote Sensing of Environment*, *130*, 280–293.

Kuemmerle, T., Hostert, P., Radeloff, V. C., Perzanowski, K., & Kruhlov, I. (2007). Post-socialist forest disturbance in the Carpathian border region of Poland, Slovakia, and Ukraine. *Ecological Applications*, *17*, 1279–1295.

Lhermitte, S., Verbesselt, J., Verstraeten, W. W., Veraverbeke, S., & Coppin, P. (2011). Assessing intra-annual vegetation regrowth after fire using the pixel based regeneration index. *ISPRS Journal of Photogrammetry and Remote Sensing*, *66*, 17–27.

Liang, S. L., Fang, H. L., Chen, M. Z., Shuey, C. J., Walthall, C., Daughtry, C., et al. (2002). Validating MODIS land surface reflectance and albedo products: Methods and preliminary results. *Remote Sensing of Environment*, *83*, 149–162.

Lu, D., Mausel, P., Brondizio, E., & Moran, E. (2004). Change detection techniques. *International Journal of Remote Sensing*, *25*, 2365–2407.

Lunetta, R. S., Knight, J. F., Ediriwickrema, J., Lyon, J. G., & Worthy, L. D. (2006). Land-cover change detection using multi-temporal MODIS NDVI data. *Remote Sensing of Environment*, *105*, 142–154.

Masek, J. G., Huang, C. Q., Wolfe, R., Cohen, W., Hall, F., Kutler, J., et al. (2008). North American forest disturbance mapped from a decadal Landsat record. *Remote Sensing of Environment*, *112*, 2914–2926.

Moody, A., & Woodcock, C. E. (1994). Scale-dependent errors in the estimation of land-cover proportions — Implications for global land-cover datasets. *Photogrammetric Engineering and Remote Sensing*, *60*(5), 585–594.

Nishihama, M., Wolfe, R., Solomon, D., Patt, F., Blanchette, J., Fleig, A., et al. (1997). *MODIS level 1A earth location: Algorithm theoretical basis document, version 3.0.* MODIS science data support team. NASA/Goddard Space Flight CenterGreenbelt, MD.

Olofsson, P., Foody, G. M., Stehman, S. V., & Woodcock, C. E. (2013). Making better use of accuracy data in land change studies: Estimating accuracy and area and quantifying uncertainty using stratified estimation. *Remote Sensing of Environment*, *129*, 122–131.

Olofsson, P., Kuemmerle, T., Griffiths, P., Knorn, J., Baccini, A., Gancz, V., et al. (2011). Carbon implications of the forest restitution in post-socialist Romania. *Environmental Research Letters*, *6*, 045202.

Pouliot, D., Latifovic, R., Fernandes, R., & Olthof, I. (2009). Evaluation of annual forest disturbance monitoring using a static decision tree approach and 250 m MODIS data. *Remote Sensing of Environment*, *113*, 1749–1759.

Roman, M. O., Schaaf, C. B., Lewis, P., Gao, F., Anderson, G. P., Privette, J. L., et al. (2010). Assessing the coupling between surface albedo derived from MODIS and the fraction of diffuse skylight over spatially-characterized landscapes. *Remote Sensing of Environment*, *114*(4), 738–760.

Roy, D. P. (2000). The impact of misregistration upon composited wide field of view satellite data and implications for change detection. *IEEE Transactions on Geoscience and Remote Sensing*, *38*, 2017–2032.

Roy, D. P., Jin, Y., Lewis, P. E., & Justice, C. O. (2005). Prototyping a global algorithm for systematic fire-affected area mapping using MODIS time series data. *Remote Sensing of Environment*, *97*, 137–162.

Roy, D. P., Ju, J., Lewis, P. E., Schaaf, C. B., Gao, F., Hansen, M., et al. (2008). Multi-temporal MODIS-Landsat data fusion for relative radiometric normalization, gap filling, and prediction of Landsat data. *Remote Sensing of Environment*, *112*, 3112–3130.

Schaaf, C. B., Gao, F., Strahler, A. H., Lucht, W., Li, X. W., Tsang, T., et al. (2002). First operational BRDF, albedo nadir reflectance products from MODIS. *Remote Sensing of Environment*, *83*, 135–148.

Shimabukuro, Y. E., Duarte, V., Anderson, L. O., Valeriano, D. M., Arai, E., Freitas, R. M., et al. (2006). Near real time detection of deforestation in the Brazilian Amazon using MODIS imagery. *Revista Ambiente e Água*, *1*, 37–47.

Singh, A. (1989). Digital change detection techniques using remotely-sensed data. *International Journal of Remote Sensing*, *10*, 989–1003.

Spruce, J. P., Sader, S., Ryan, R. E., Smoot, J., Kuper, P., Ross, K., et al. (2011). Assessment of MODIS NDVI time series data products for detecting forest defoliation by gypsy moth outbreaks. *Remote Sensing of Environment*, *115*, 427–437.

Tan, B., Woodcock, C. E., Hu, J., Zhang, P., Ozdogan, M., Huang, D., et al. (2006). The impact of gridding artifacts on the local spatial properties of MODIS data: Implications for validation, compositing, and band-to-band registration across resolutions. *Remote Sensing of Environment*, *105*, 98–114.

Townshend, J. R. G., Huang, C., Kalluri, S. N. V., Defries, R. S., Liang, S., & Yang, K. (2000). Beware of per-pixel characterization of land cover. *International Journal of Remote Sensing*, *21*, 839–843.

Townshend, J. R. G., & Justice, C. O. (1988). Selecting the spatial resolution of satellite sensors required for global monitoring of land transformations. *International Journal of Remote Sensing*, *9*, 187–236.

Verbesselt, J., Zeileis, A., & Herold, M. (2012). Near real-time disturbance detection using satellite image time series. *Remote Sensing of Environment*, *123*, 98–108.

Wolfe, R. E., Nishihama, M., Fleig, A. J., Kuyper, J. A., Roy, D. P., Storey, J. C., et al. (2002). Achieving sub-pixel geolocation accuracy in support of MODIS land science. *Remote Sensing of Environment*, *83*, 31–49.

Wolfe, R. E., Roy, D. P., & Vermote, E. (1998). MODIS land data storage, gridding, and compositing methodology: Level 2 grid. *IEEE Transactions on Geoscience and Remote Sensing*, *36*, 1324–1338.

WWW1 (n.d). The USGS Global Visualization Viewer. http://glovis.usgs.gov

WWW2 (n.d). Web of Level 1 and Atmosphere Archive and Distribution System (LAADS). http://ladsweb.nascom.nasa.gov/data/search.html

WWW3 (n.d). The Reverb Tool in Land Processes Distributed Active Archive Center (LPDAAC). http://reverb.echo.nasa.gov/reverb/

WWW4 (n.d). The BRDF Forward Model Tool. http://www-modis.bu.edu/brdf/userguide/tools.html

WWW5 (n.d). The MODIS Reprojection Tool. https://lpdaac.usgs.gov/lpdaac/tools/modis_reprojection_tool

Zhan, X., Sohlberg, R. A., Townshend, J. R. G., DiMiceli, C., Carroll, M. L., Eastman, J. C., et al. (2002). Detection of land cover changes using MODIS 250 m data. *Remote Sensing of Environment*, *83*, 336–350.

Zhu, Z., Woodcock, C. E., & Olofsson, P. L. (2012). Continuous monitoring of forest disturbance using all available Landsat imagery. *Remote Sensing of Environment*, *122*, 75–91.

View publication stats